Supporting Information: Mechanistic insight into the framework methylation of H-ZSM-5 for varying methanol loading and Si/Al ratio using first principles molecular dynamics simulation

Stefan A. F. Nastase [1], Pieter Cnudde [2,*], Louis Vanduyfhuys [2], Kristof De Wispelaere [2], Veronique Van Speybroeck [2], C. Richard A. Catlow[1,3,4], Andrew J. Logsdail[1,*]

1 Cardiff Catalysis Institute, School of Chemistry, Cardiff University, CF10 3AT, UK

2 Center for Molecular Modeling, Ghent University, Zwijnaarde, Belgium

3 Department of Chemistry, University College London, 20 Gordon St., London WC1E 6BT, UK

4 UK Catalysis Hub, Research Complex at Harwell, Science and Technology Facilities Council, Rutherford Appleton Laboratory, Oxford, OX11 0FA, UK

* *pieter.cnudde@ugent.be*, *LogsdailA@cardiff.ac.uk*

Overview

Section S1. MD simulations cell parameters.

Section S2. Methanol loading per pore volume analysis

Section S3. Geometric analysis of MD simulations.

Section S4. MTD cell parameters and analysis of methodology employed

Section S5. QM/MM geometry optimisation of single methanol adsorption

Section S6. Time dependent variation of M-A and M-R distances

Section S7. Kinetic and FES results.

Section S1. MD simulations cell parameters

The unit cell parameters (Table S1) were averaged from NPT equilibration simulations, and then carried forward to our NVT simulations.

Table S1. Cell parameters of NPT simulations at 300 K and 1 atm specific to the Si/Al ratio of simulation models (top three rows), given in Å and °, compared to experimental values (bottom row).

Si/Al	a (Å)	b (Å)	c (Å)	α (°)	β (°)	γ (°)
95	20.05	19.85	13.38	90.87	90.42	90.28
95*	20.09	19.92	13.40	90.02	90.01	90.11
47	20.05	19.84	13.43	91.16	89.80	89.92
299[1]	20.02	19.90	13.38	90.00	90.00	90.00

** Parameters used for MD simulation at 670 K of 5 methanol molecules per one acid site unit cell.*

Section S2. Methanol loading per pore volume analysis

The Zeo++ package[2] was used to evaluate the available space within the H-ZSM-5 framework that could accommodate guest molecules (Figure S1). The pore-occupiable volume implemented in Zeo++ was used as an estimate for the available space. This analysis includes both channels and intersections within the zeolite framework.

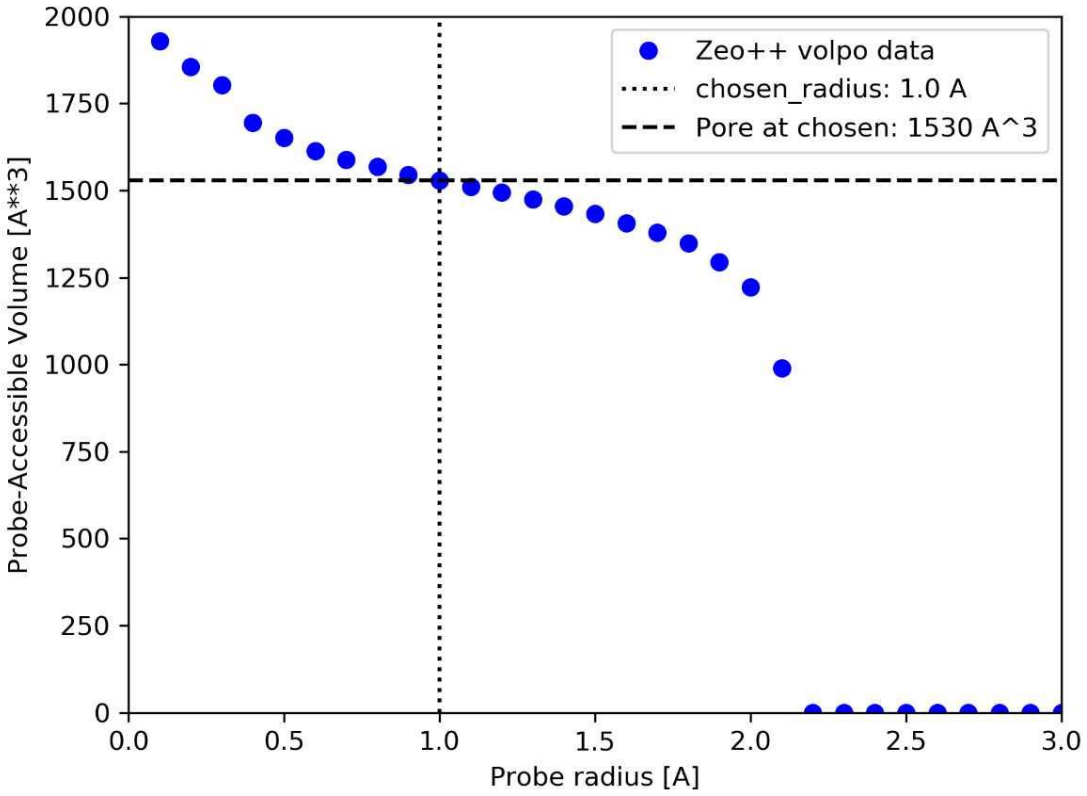

Figure S1. Plot of the accessible space within the entire zeolite unit cell of ZSM-5 against guest molecule radius, given in Å^3 and Å, respectively.

We use as an approximate probe radius of the methanol molecule as 1 Å, which allows us to estimate the number of methanol molecules that can be inserted in the zeolite model while avoiding sampling of the space in between atoms or small cages.

Considering the adsorption energy of a single methanol molecule within the zeolite, which falls between -90 and -115 kJ/mol in previous work, one can evaluate the loading of the pore with methanol (Figure S2)[3]. The relatively large adsorption energy of methanol to the Brønsted acid site resulted in a high saturation, with up to 13 methanol molecules around one active site, however this may be overestimated since the adsorption is assumed to be homogenous throughout the entire pore volume. High quantity of up to 11 methanol molecules coordinating with one acid site is also observed experimentally[4].

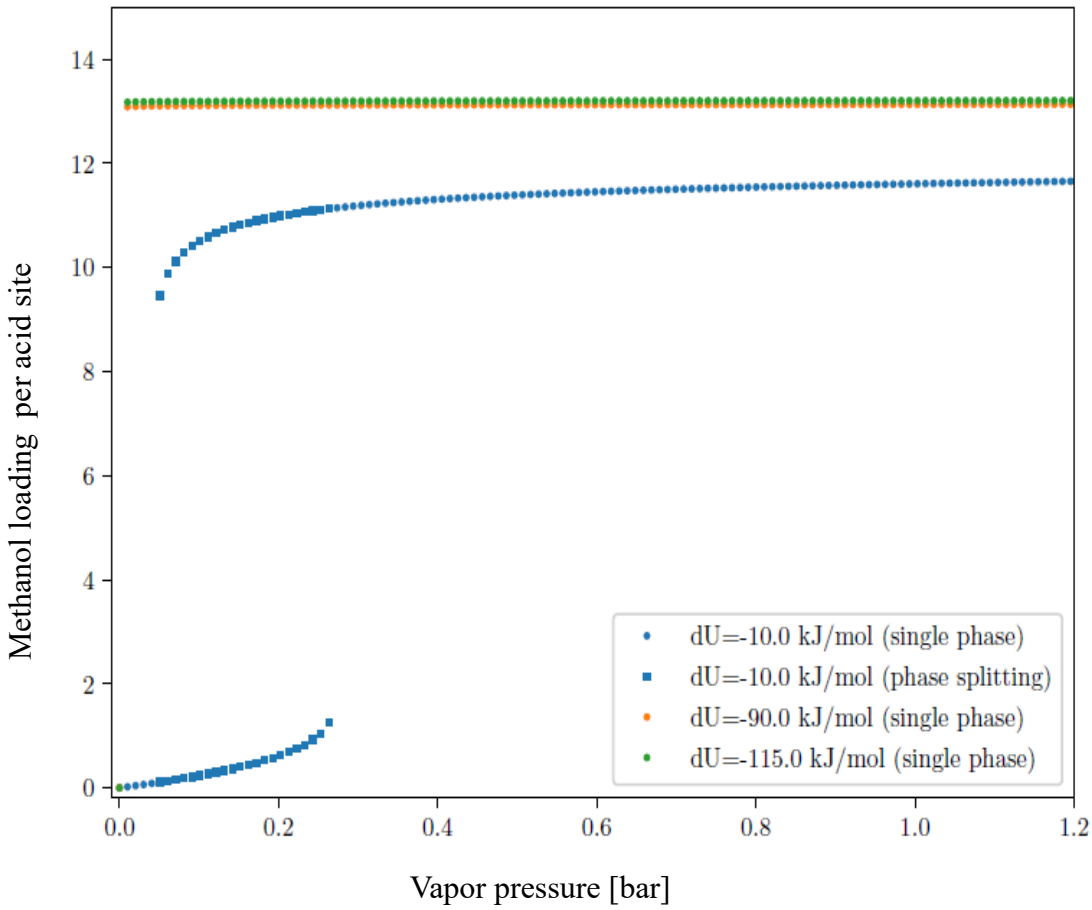

Figure S2. Methanol loading per acid site as a function of the methanol vapor pressure. A key is provided.

Section S3. Geometric analysis of MD simulations

Table S2. Minimum, average and maximum intermolecular distances, d, between methanol molecules of interest throughout the NVT simulations. In particular, we present distances between methyl groups (C_M-C_M), oxygen atoms of methanol molecules (O_M-O_M). Schematic representation of the analysed intermolecular distances given in Figure 1 of article. Distances are given in Å.

Methanol/cell		3 MeOH		5 MeOH				
Si/Al ratio		95	47	95	47			
$d(C_{M1}$-$C_{M2})$	min.	3.18	3.31	3.46	3.64	-	-	-
	ave.	4.38	4.25	4.47	4.52			
	max.	4.96	5.05	5.43	5.08	-	-	-
$d(C_{M2}$-$C_{M3})$	min.	3.25	3.24	3.32	2.81	-	-	-
	ave.	4.27	4.28	4.10	3.40			
	max.	5.17	5.48	4.87	4.06	-	-	-
$d(C_{M3}$-$C_{M4})$	min.	-	-	3.14	-	-	-	-
	ave.			4.45				
	max.	-	-	5.69	-	-	-	-
$d(C_{M4}$-$C_{M5})$	min.	-	-	2.93	-	-	-	-
	ave.			3.87				
	max.	-	-	4.96	-	-	-	-
Methanol/cell		1 MeOH			3 MeOH		5 MeOH	
Si/Al ratio		95	47	47*	95	47	95	47
$d(O_{M1}$-$O_{M2})$	min.	-	-	-	2.25	2.25	2.28	2.26
	ave.				2.45	2.51	2.60	2.47
	max.	-	-	-	2.94	3.27	3.17	2.99
$d(O_{M2}$-$O_{M3})$	min.	-	-	-	2.29	2.27	2.25	2.29
	ave.				2.59	2.53	2.47	2.59
	max.	-	-	-	3.15	3.43	2.89	3.20
$d(O_{M3}$-$O_{M4})$	min.	-	-	-	-	-	2.26	-
	ave.						2.56	
	max.	-	-	-	-	-	3.16	-
$d(O_{M4}$-$O_{M5})$	min.	-	-	-	-	-	2.34	-
	ave.						2.83	
	max.	-	-	-	-	-	3.55	-

"-" no results to present

*Results of methanol adsorbed on T8 acid site instead of T12.

Table S3. Minimum and maximum intermolecular hydrogen bond distances, d(O_M-H), in methanol molecules of interest (Å), taken over from our NVT simulations. Schematic representation of the analysed intermolecular distances given in Figure 1 of article.

Methanol/cell		1 MeOH			3 MeOH		5 MeOH	
Si/Al ratio		95	47	47*	95	47	95	47
d(H_{M1}-O_{M1})	min.	0.95	0.90	0.90	0.90	0.90	0.88	0.90
	max.	1.91	1.77	1.75	1.35	1.28	1.21	1.36
d(O_{M1}-H_{M2})	min.	-	-	-	0.96	0.94	0.97	0.93
	max.	-	-	-	1.99	2.56	2.35	2.21
d(H_{M2}-O_{M2})	min.	-	-	-	0.94	0.93	0.92	0.91
	max.	-	-	-	1.79	1.75	1.59	1.90
d(O_{M2}-H_{M3})	min.	-	-	-	0.91	0.93	0.93	0.91
	max.	-	-	-	1.56	1.72	2.01	1.53
d(H_{M3}-O_{M3})	min.	-	-	-	1.03	0.99	0.93	1.00
	max.	-	-	-	2.23	2.66	1.83	2.33
d(H_{M3}-O_{M4})	min.	-	-	-	0.85	0.90	0.92	0.82
	max.	-	-	-	1.25	1.20	1.63	1.29
d(H_{M4}-O_{M4})	min.	-	-	-	-	-	0.94	-
	max.	-	-	-	-	-	2.51	-
d(O_{M4}-H_{M5})	min.	-	-	-	-	-	0.87	-
	max.	-	-	-	-	-	1.35	-
d(H_{M5}-O_{M5})	min.	-	-	-	-	-	1.14	-
	max.	-	-	-	-	-	3.05	-
d(O_{M5}-H_{M6})	min.	-	-	-	-	-	0.81	-
	max.	-	-	-	-	-	1.29	-

"-" no results to present

*Results of methanol adsorbed on T8 acid site instead of T12.

Section S4. MTD cell parameters and analysis of methodology employed

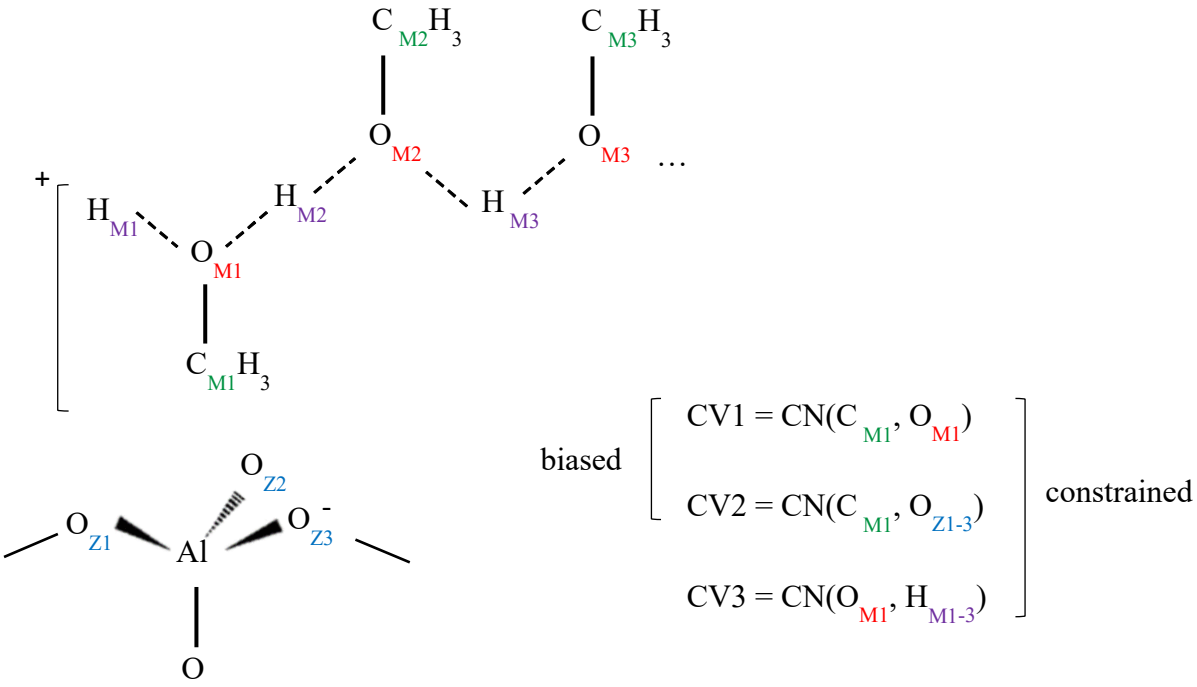

Figure S3. Schematic representation of the CVs employed in Metadynamics simulations.

Upon each recrossing of the barrier, the height of the Gaussian hills is halved in order to improve the convergence of the free energy profile; this process is repeated until a final hill height of 0.65 kJ/mol is used. To ensure we sample chemically relevant space with the metadynamics simulations, we use constraints to keep the reactant and product molecules in the vicinity of the acid site. In particular, we constrain the C-O bonds represented by CV1 and CV2 to the reaction transition state by using a series of single-sided energy "walls", that extend from the barrier (B) towards smaller values of the collective variable (CV), represented by a quadratic potential $K(CV-B)^2$, with K - quadratic potential constant: for CV1, this barrier is at $CN(C_{MeOH}\text{-}O_{MeOH}) = 0.04$ (K=50 Ha), which corresponds to a bond distance of 3.4 Å; and for CV2, the barrier is at $CN(C_{MeOH}\text{-}O_{zeolite}) = 0.03$ (K=200 Ha). In addition, to keep the reactant methanol protonated, which we observe as an active part of the reaction mechanism when more than one methanol is adsorbed on the active site, we applied a quadratic wall in position 0.056 of CV3 (K=100 Ha), which corresponds to an average O-H stretch of 1.25 Å and a maximum elongation from the the methanol of 2 Å; this parameter choice is based on the average O-H bond lengths observed for the protonated methanol in our NPT simulations.

For metadynamics simulations, it is necessary to use unit cells equilibrated in the NPT ensemble with the appropriate methanol loading from the outset (Table S4). Furthermore, the average O-H bond distance for the methoxonium ion is also presented in Table S5. An overview of all the simulated models is presented in Table S6.

Table S4. Average unit cell parameters observed during NPT simulations with methanol loaded into the unit cell. These parameters were subsequently used for metadynamics simulations. Lattice vectors and angles are given in Å and °, respectively.

Si/Al	Methanol/cell	a (Å)	b (Å)	c (Å)	α (°)	β (°)	γ (°)
95	1 MeOH	20.05	19.79	13.41	91.24	90.63	90.24
47		20.04	19.86	13.39	90.90	90.59	90.30
95	3 MeOH	19.96	19.80	13.27	90.14	90.20	90.35
47		20.03	19.84	13.38	90.91	89.89	90.15
95	5 MeOH	20.02	19.81	13.38	91.03	90.36	90.20
47		20.05	19.82	13.38	91.13	90.14	90.15

Table S5. Average O-H distance observed for the protonated methanol in our NPT equilibration calculations. Values are given in Å.

Si/Al	Methanol/cell	d(O-H)
95	3 MeOH	1.24
47		1.13
95	5 MeOH	1.19
47		1.16

Table S6. Overview of models employed for MD and MTD simulations, with methanol and Si/Al ration presented alongside simulation time given in picoseconds (ps) and meta-picoseconds (m-ps)

MD. NPT*			MD. NVT		
Si/Al	Methanol loading	time [ps]	Si/Al	Methanol loading	time [ps]
95	1	50	95	1	50
95	3	50	95	3	50
95	5	50	95	5	50
47	1	50	47	1	50
47	3	50	47**	3	50
47	5	50	47	5	50
Metadynamics					
Si/Al	Methanol loading	time [m-ps]			
95	1	277			
95	3	231			
95	5	213			
47	1	223			
47	3	184			
47	5	196			

** Two MD, NPT runs were simulated in parallel for each model, to ensure a proper sampling process occurred.*

*** Two distinct configurations were simulated for the MD, NVT 3 methanol, 2 acid sites per unit cell models.*

To validate our method and parameters for the metadynamics simulations themselves, multiple simulations were conducted to obtain accurate parameters. To perform this validation, the unit cell chosen was a zeolite model containing three methanol molecules and one acid site. In order to ensure that no different reaction path is taken when employing two CVs, the accuracy behind using two CVs was analysed by conducting a MTD simulation having a single biased CV: CN1-CN2 or the difference between the coordination number of the methyl to the oxygen of the methanol hydroxyl – (CV1) and the coordination number of the as methyl to the oxygen atoms of the active site–(CV2), as shown in the Methodology section of the article.

With respect to the refinement of the energy landscape and the Gaussian "hills" added when sampling, it was concluded that a "hill" height of 0.65 kJ/mol was adequate; subsequent refinement with energy hills of 0.30 kJ/mol and 0.10 kJ/mol, both of which were performed for an additional 25 ps (corresponding to 500 energy hills added for each energy "layer") did

not give a statistically significant change in the minimum energy path (MEP) free energy barrier (Table S7).

Table S7. MEP free energy barriers calculated from metadynamics simulation with two collective variables biased - MTD (CN1, CN2), one collective variable biased (CN1-CN2). Values are presented in kJ/mol.

	"Hill" height:		
	0.65	0.30	0.10
MTD (CN1, CN2)	169	166	165
MTD (CN1 - CN2)	171	-	-

"-" no results to present

Section S5. QM/MM geometry optimisation of single methanol adsorption

To further validate that single methanol adsorption can lead to acid site deprotonation, an additional set of simulations was performed by taking an MD snapshot from a single acid site per unit cell production run, in which the acid site was deprotonated, as the starting geometry. This model was geometrically optimised using QM/MM static calculations, which resulted in the methanol being in a protonated state (Figure S3) thus validating that the PES contains local minimums in which the acid site is deprotonated.

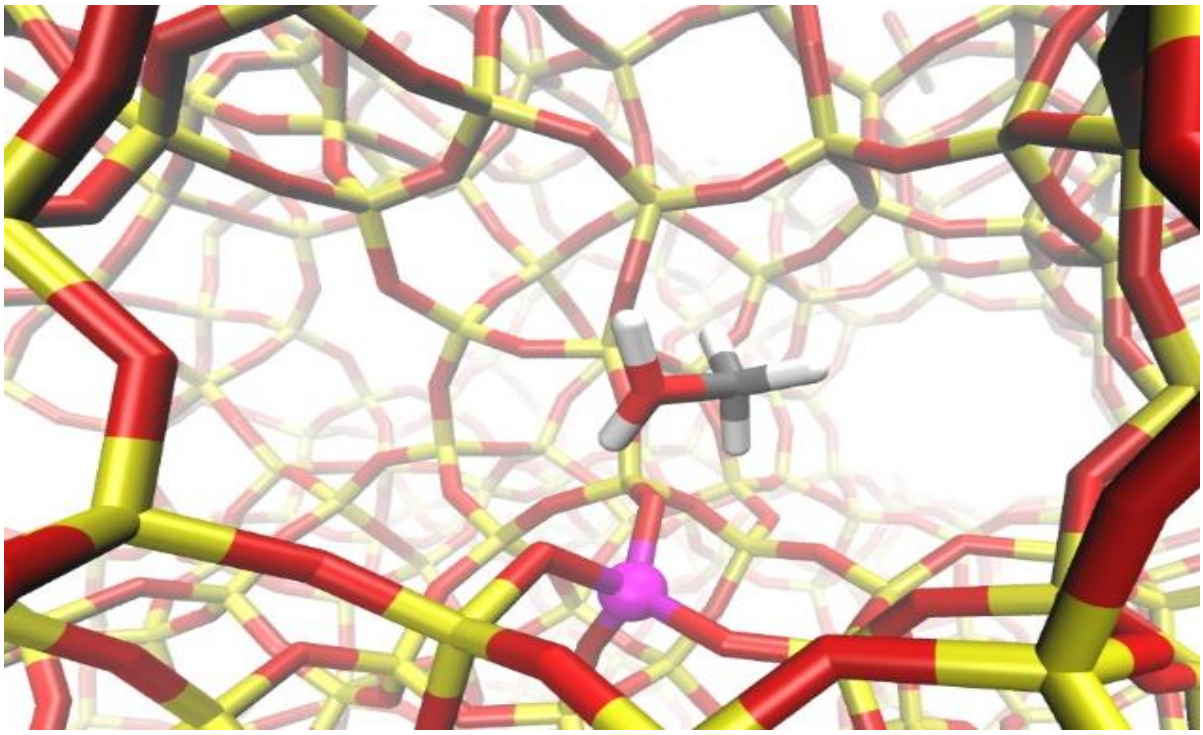

Figure S4. QM/MM optimised model of single methanol adsorption on T12 acid site, with atoms colour key as described in Figure 3 in the main article.

To perform the QM/MM calculations, we created spherical embedded-cluster models of H-ZSM-5 from the experimental unit cells of siliceous MFI[5], centred on a T12 Si tetrahedral in the intersection channel. During QM calculations, the terminal oxygens are saturated with hydrogen atoms: these artificial "link" atoms do not inadvertently affect the electronic solution of the QM calculations, as a bond-dipole correction is added at the boundary to the surrounding MM region, to ensure an accurate electrostatic embedding potential.[6] Encapsulating the QM region are two concentric MM regions. The inner MM region contains atoms that can move during a geometry optimisation; and the outer region is frozen to ensure a bulk-like structure at the far limit from any chemical reactions. In our calculations, the inner and outer MM regions extend from the central T-site to a radius of 10.58 Å (20 a_0) and 21.17 Å (40 a_0), respectively.

Surrounding the entire QM/MM cluster is a series of embedding point charges, the values of which have been fitted to give the correct bulk electrostatic potential for all the sites allowed to move during any geometry optimisation (*i.e*. the QM and inner MM region), as referenced against a periodic MM calculation for the same system.[7, 8]

After creating our embedded-cluster model, we replaced the central Si atom in each model with an Al atom, and have added a charge compensating H on a neighbouring oxygen atom in a manner that facilitates reaction modelling, specifically where the H atom is most accessible, noting that the energy differences between H locations are typically small[9,10,11]. The QM region, which is the chemically active part of our model, includes atoms up to the fifth nearest neighbour (the third oxygen atom) from the central T-site. In their entirety, the total number of atoms in each cluster model is 2165, with 74 QM atoms and 197 inner MM atoms.

Throughout, the QM energy has been calculated using hybrid-DFT with the Becke97-3 exchange-correlation (XC) functional[12], using the dispersion corrected B97-D version[13], as provided in the NWChem code[14]. Throughout, the atomic orbitals are represented using the Ahlrichs and Taylor TZVP Gaussian basis sets[15]. The self-consistent field (SCF) convergence criteria was set to an energy change of less than 2.72×10^{-6} eV (1×10^{-7} Hartrees) between SCF iterations.[16,17] The MM energy was calculated using DL_POLY,[18] employing the forcefield of Hill and Sauer[7,8], with the coordination dependent charges in the original forcefield replaced with fixed 1.2 and -0.6 e point charges for silicon and oxygen respectively, as parameterised in the work of Sherwood *et al.*[6] Because we have a neutrally charged system, we employed Restricted Hartree-Fock (RHF) conditions to simulate our models, corresponding to all spins being paired and singlet spin multiplicity. Geometry optimizations were performed by ChemShell[19] in a Cartesian coordinate space using the Limited-Memory Broyden-Fletcher-Goldfarb-Shanno (L-BFGS) algorithm, with a convergence threshold of 0.015 eV/Å, gradients of root-mean-square (rms) of 0.002 Ha/a_0, rms of 0.008 a_0, maximum gradient of 0.003 Ha/a_0, maximum displacement of 0.012 a_0.[20,21,22,23] Vibrational frequencies were also calculated using ChemShell, with a task-farmed finite-difference approach, [24] allowing us to confirm that the geometry corresponds to local minima.[25,26]

Section S6. Time dependent variation of M-A and M-R distances

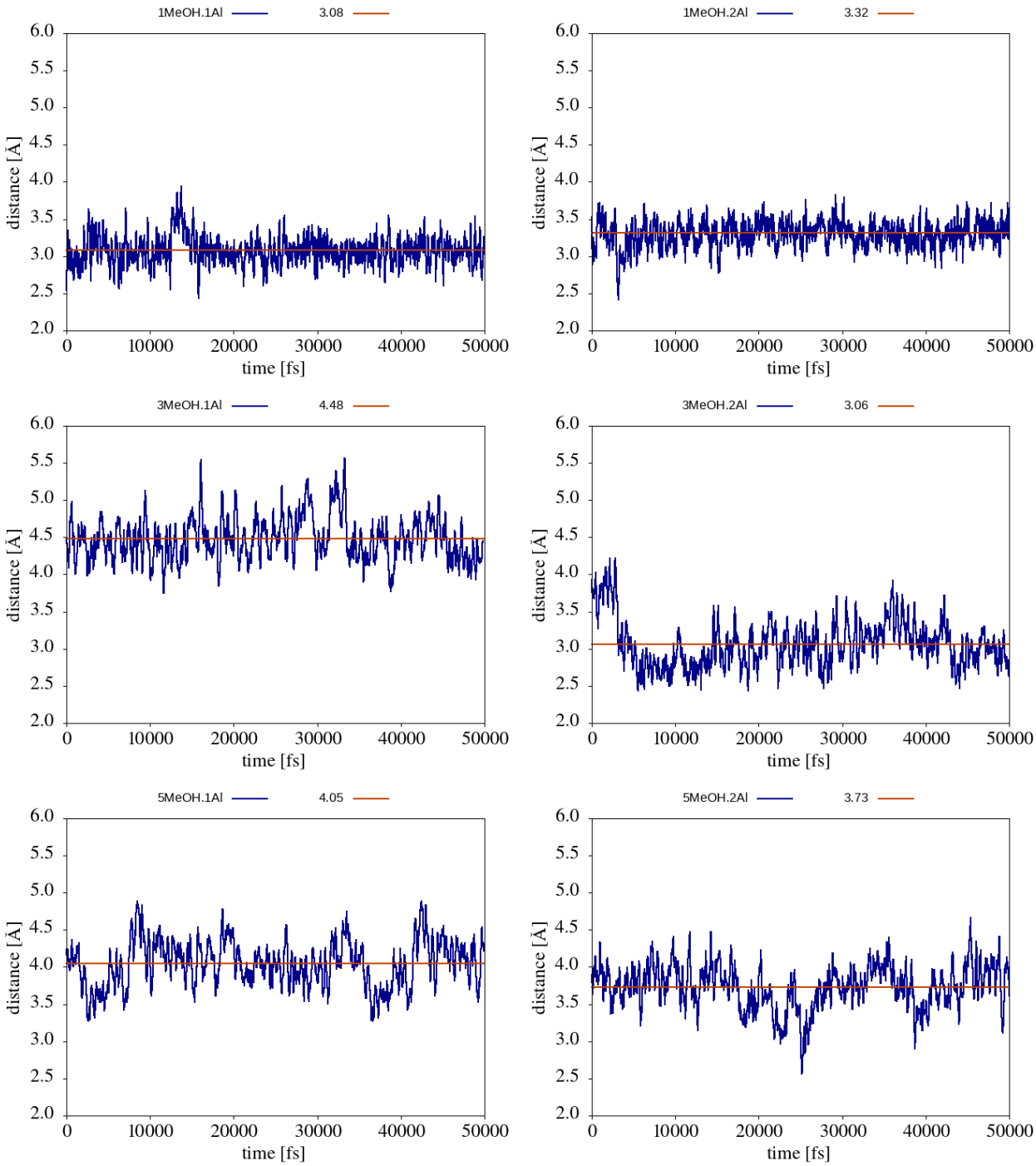

Figure S5. Variation of M-A distance (Å) as a function of simulation time (fs) for a 50 ps NVT simulation. Data is presented for one (top row) and two (bottom row) acid sites, with one (left column), three (middle column) and five (right column) methanol molecules per unit. The orange horizontal line highlights the average distance.

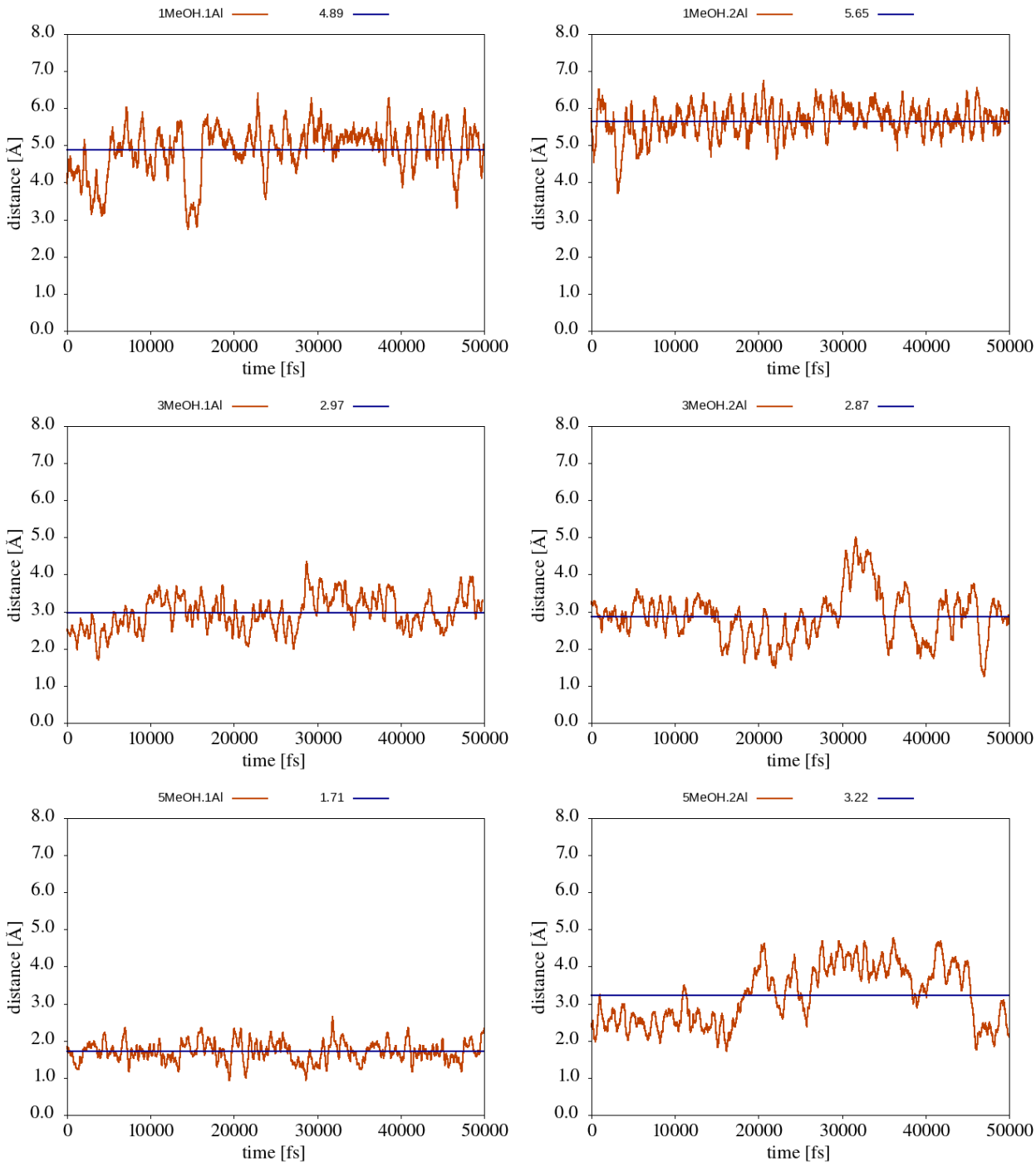

Figure S6. Variation of M-R distance (Å) as a function of simulation time (fs) in a 50 ps NVT simulation. Data is presented for one (top row) and two (bottom row) acid sites, with one (left column), three (middle column) and five (right column) methanol molecules per unit cell. A blue horizontal line highlights the average distance.

Table S8. Average distances of M-A and M-R from NVT MD simulations, given in Å. The definitions of M, A and R are given in the manuscript Methodology.

Si/Al ratio	Methanol/cell	*M-A*	*M-R*
95	1 MeOH	3.08	4.89
47		3.32	5.65
95	3 MeOH	4.48	2.97
47		3.06	2.87
95	5 MeOH	4.05	1.71
47		3.73	3.22

Section S7. Kinetic and FES results.

The methylation reaction rate constants (k) are calculated as follows:

$$k = A\left(\frac{e^{-\beta F(q*)}}{\bar{Z}R}\right) \quad (1)$$

with $F(q^*)$ representing the free energy of the transition state q^*, which is relative to the energy minimum in the reactant "valley"; $\bar{Z}_R$ is proportional to the partition function of the reactant "valley"; and A is a factor related to rate of change of the collective variable in the transition state and was computed by the procedure proposed by Bučko *et al*[27].

Table S9. Kinetic properties and MEP barriers derived from the FES analysis, specifically, free energy barriers of the forward reaction (ΔF_F), backward reaction (ΔF_B) presented in kJ/mol, reaction rates of the forward (k_F) and backward reactions (k_B) (given in s^{-1}), calculated as provided in the methodology section of main article.

		Phenomenological barriers		Kinetic rates	
Si/Al ratio	Methanol/u.c.	ΔF_F	ΔF_B	k_F	k_B
95	1 MeOH	142	98	$7.37\cdot10^{-13}$	$1.22\cdot10^{-2}$
95	3 MeOH	169	55	$1.94\cdot10^{-17}$	$1.66\cdot10^{3}$
47		142	79	$1.38\cdot10^{-12}$	$1.13\cdot10^{-1}$
95	5 MeOH	149	44	$6.24\cdot10^{-14}$	$1.22\cdot10^{5}$
47		112	66	$1.73\cdot10^{-7}$	$1.73\cdot10$

References:

(1) Van Koningsveld, H.; Van Bekkum, H.; Jansen, J. C. On the Location and Disorder of the Tetrapropylammonium (TPA) Ion in Zeolite ZSM-5 with Improved Framework Accuracy. *Acta Crystallogr. Sect. B* **1987**, *B43*, 127.

(2) Willems, T. F.; Rycroft, C. H.; Kazi, M.; Meza, J. C.; Haranczyk, M. Algorithms and Tools for High-Throughput Geometry-Based Analysis of Crystalline Porous Materials. *Microporous Mesoporous Mater.* **2012**, *149* (1), 134–141.

(3) Vanduyfhuys, L.; Ghysels, A.; Rogge, S. M. J.; Demuynck, R.; Speybroeck, V. V. Semi-Analytical Mean-Field Model for Predicting Breathing in Metal–Organic Frameworks. *Mol. Simul.* **2015**, *41* (16–17), 1311–1328.

(4) Omojola, T.; Cherkasov, N.; McNab, A. I.; Lukyanov, D. B.; Anderson, J. A.; Rebrov, E. V.; van Veen, A. C. Mechanistic Insights into the Desorption of Methanol and Dimethyl Ether Over ZSM-5 Catalysts. *Catal. Lett.* **2018**, *148* (1), 474–488.

(5) Artioli, G.; Lamberti, C.; Marra, G. L. Neutron Powder Diffraction Study of Orthorhombic and Monoclinic Defective Silicalite. *Acta Crystallogr. B* **2000**, *56* (1), 2–10.

(6) Sherwood, P.; De Vries, A. H.; Collins, S. J.; Greatbanks, S. P.; Burton, N. A.; Vincent, M. A.; Hillier, I. H. Computer Simulation of Zeolite Structure and Reactivity Using Embedded Cluster Methods. *Faraday Discuss* **1997**, *106*, 79–92.

(7) Hill, J. R.; Sauer, J. Molecular Mechanics Potential for Silica and Zeolite Catalysts Based on Ab Initio Calculations. 1. Dense and Microporous Silica. *J. Phys. Chem.* **1994**, *98* (4), 1238–1244.

(8) Hill, J.-R.; Sauer, J. Molecular Mechanics Potential for Silica and Zeolite Catalysts Based on Ab Initio Calculations. 2. Aluminosilicates. *J. Phys. Chem.* **1995**, *99* (23), 9536–9550.

(9) O'Malley, A. J.; Logsdail, A. J.; Sokol, A. A.; Catlow, C. R. A. Modelling Metal Centres, Acid Sites and Reaction Mechanisms in Microporous Catalysts. *Faraday Discuss* **2016**, *188*, 235–255.

(10) Sastre, G.; Fornes, V.; Corma, A. On the Preferential Location of Al and Proton Siting in Zeolites: A Computational and Infrared Study. *J. Phys. Chem. B* **2002**, *106* (3), 701–708.

(11) Ghorbanpour, A.; Rimer, J. D.; Grabow, L. C. Periodic, VdW-Corrected Density Functional Theory Investigation of the Effect of Al Siting in H-ZSM-5 on Chemisorption Properties and Site-Specific Acidity. *Catal. Commun.* **2014**, *52*, 98–102.

(12) Keal, T. W.; Tozer, D. J. Semiempirical Hybrid Functional with Improved Performance in an Extensive Chemical Assessment. *J. Chem. Phys.* **2005**, *123* (12).

(13) Grimme, S. Semiempirical GGA-Type Density Functional Constructed with a Long-Range Dispersion Correction. *J. Comput. Chem.* **2006**, *27* (15), 1787–1799.

(14) Valiev, M.; Bylaska, E. J.; Govind, N.; Kowalski, K.; Straatsma, T. P.; Van Dam, H. J. J.; Wang, D.; Nieplocha, J.; Apra, E.; Windus, T. L.; De Jong, W. A. NWChem: A

Comprehensive and Scalable Open-Source Solution for Large Scale Molecular Simulations. *Comput. Phys. Commun.* **2010**, *181* (9), 1477–1489.

(15) Ahlrichs, R.; Taylor, P. R. The Choice of Gaussian Basis Sets for Molecular Electronic Structure Calculations. *J Chim Phys* **1981**, *78*, 315–324.

(16) Hartree, D. R. The Wave Mechanics of an Atom with a Non-Coulomb Central Field.Part I. Theory and Methods. *Math. Proc. Camb. Philos. Soc.* **1928**, *24* (03), 426.

(17) Fock, V. Näherungsmethode Zur Losung Des Quantenmechanischen Mehrkorperproblems. *Z. Phys.* **1930**, *61* (1–2), 126–148.

(18) Smith, W.; Yong, C. W.; Rodger, P. M. DL_POLY: Application to Molecular Simulation. *Mol. Simul.* **2002**, *28*, 37–41.

(19) Metz, S.; Kästner, J.; Sokol, A. A.; Keal, T. W.; Sherwood, P. ChemShell-a Modular Software Package for QM/MM Simulations. *Wiley Interdiscip. Rev. Comput. Mol. Sci.* **2014**, *4* (2), 101–110.

(20) Broyden, C. G. The Convergence of Single-Rank Quasi-Newton Methods. *Math. Comput.* **1970**, *24* (110), 365–365.

(21) Fletcher, R. A New Approach to Variable Metric Algorithms. *Comput. J.* **1970**, *13* (3), 317–322.

(22) Goldfarb, D. A Family of Variable-Metric Methods Derived by Variational Means. *Math. Comput.* **1970**, *24* (109), 23–23.

(23) Shanno, D. F. Conditioning of Quasi-Newton Methods for Function Minimization. *Math. Comput.* **1970**, *24* (111), 647–647.

(24) Guest, M. F.; Bush, I. J.; Van Dam, H. J.; Sherwood, P.; Thomas, J. M. H.; Van Lenthe, J. H.; Havenith, R. W.; Kendrick, J. The GAMESS-UK Electronic Structure Package: Algorithms, Developments and Applications. *Mol. Phys.* **2005**, *103* (6–8), 719–747.

(25) Swope, W. C.; Andersen, H. C.; Berens, P. H.; Wilson, K. R. A Computer Simulation Method for the Calculation of Equilibrium Constants for the Formation of Physical Clusters of Molecules: Application to Small Water Clusters. *J. Chem. Phys.* **1982**, *76* (1), 637–649.

(26) Kästner, J.; Carr, J. M.; Keal, T. W.; Thiel, W.; Wander, A.; Sherwood, P. DL-FIND: An Open-Source Geometry Optimizer for Atomistic Simulations. *J. Phys. Chem. A* **2009**, *113* (43), 11856–11865.

(27) Bučko, T.; Chibani, S.; Paul, J.-F.; Cantrel, L.; Badawi, M. Dissociative Iodomethane Adsorption on Ag-MOR and the Formation of AgI Clusters: An Ab Initio Molecular Dynamics Study. *Phys. Chem. Chem. Phys.* **2017**, *19* (40), 27530–27543.